Stabilization of the ferroelectric phase and relaxor-like behaviour in low Li content sodium niobates

2004 J. Phys.: Condens. Matter 16 7493

(http://iopscience.iop.org/0953-8984/16/41/027)

INSTITUTE OF PHYSICS PUBLISHING JOURNAL OF PHYSICS: CONDENSED MATTER

J. Phys.: Condens. Matter **16** (2004) 7493–7510 PII: S0953-8984(04)76011-7

Stabilization of the ferroelectric phase and relaxor-like behaviour in low Li content sodium niobates

R Jiménez[1,3], **M L Sanjuán**[2] **and B Jiménez**[1]

[1] Instituto de Ciencia de Materiales de Madrid (ICMM), CSIC, Cantoblanco, 28049 Madrid, Spain
[2] Instituto de Ciencia de Materiales de Aragón (Universidad de Zaragoza-CSIC), Facultad de Ciencias, Universidad de Zaragoza, 50009 Zaragoza, Spain

Received 6 February 2004, in final form 21 June 2004
Published 1 October 2004
Online at stacks.iop.org/JPhysCM/16/7493
doi:10.1088/0953-8984/16/41/027

Abstract

Studies of dielectric permittivity as a function of the temperature and frequency on Li–Na niobate ceramics in the $x = 0$–5% Li compositional range have been performed. The results obtained for compositions with $0 \leqslant x \leqslant 4\%$ have revealed small wide anomalies below the temperature of the main peak corresponding to a ferroelectric (FE) or antiferroelectric (AFE)–paraelectric (PE) or antiferroelectric–antiferroelectric phase transition. The $x = 5\%$ Li composition does not show peaks below the temperature of the dielectric constant main peak. The behaviour of the real and imaginary parts of dielectric permittivity of these anomalies as a function of the temperature and measuring frequency together with their Vogel–Fulcher–Tamman like relaxation process gather the characteristics of a relaxor-like behaviour for $1 \leqslant x \leqslant 4\%$ Li-content compositions, but not in the case of $x = 0$ composition. The evolution of the Raman spectrum in the 50–180 cm^{-1} region evidences small structural changes in the 450–560 K temperature interval that indicate the coexistence of two close structural phases with similar energies that should correspond to a ferroelectric Q phase and an antiferroelectric P phase. These obtained results support the assumption of diffusive AFE–FE and FE–AFE phase transitions for $x = 0\%$ Li-content and a relaxor-like AFE–FE for $1\% \leqslant x \leqslant 4\%$ content compositions with maxima in the dielectric permittivity in that temperature interval. The results for $x = 5\%$ Li-content composition suggest that a single ferroelectric Q-like phase is stabilized. An attempt at a phase diagram is proposed.

[3] Author to whom any correspondence should be addressed.

0953-8984/04/417493+18$30.00

1. Introduction

The interest in reducing environmental pollution is leading in the case of ferro-piezoelectric material production to the search for lead free compositions that can replace in many technical applications those compositions arising from the nowadays widely extended lead titanate derived compounds. The sodium–lithium niobates in the low lithium content side of the solid solution are becoming very promising compositions to reach that objective due to their high piezoelectric coefficients.

The lithium substituted sodium niobate compounds $Li_xNa_{(1-x)}NbO_3$, hereafter referred to as LNN(x), with x as the percentage of Li content, have perovskite type structure and present several structural phase transitions of the ferroelectric–antiferroelectric [1], antiferroelectric–paraelectric [1], ferroelectric–paraelectric [2] and ferroelastic–paraelastic [3] type. Compositions with $x < 2\%$ are antiferroelectric (AFE) and those with $x \geqslant 2\%$ are ferroelectric (FE) at room temperature [2]. It has also been suggested that in pure sodium niobate LNN(0) composition fluctuations produce regions with different Na content [4] (local non-stoichiometry) giving place to the coexistence of phases, named Q, P phases, at room temperature. The transformation from the antiferroelectric P phase to the ferroelectric Q phase can be obtained by applying a strong electric field or by substitution of 2.5% K atoms for Na [5].

In the AFE phase of $NaNbO_3$ Lanfredi *et al* [6] have reported a relaxor-like phase transition at 280 K and FE–FE phase transitions have been found in compositions with $x = 2\%$ [7]—3% [8] and 12% [9], at 260–280 K on heating and at 180–190 K on cooling. Single crystal diffraction studies have proved for the $x = 2\%$ Li composition [10] to be ferroelectric along the b axis and antiferroelectric along the c axis with a crystal structure closely related to that of phase P. In $x = 3\%$ composition single crystals, it has been shown [8] that the spontaneous polarization lays in the orthorhombic b-axis direction above 280 K and in the rhombohedral c-axis direction at temperatures below 280 K.

Room temperature Raman spectra of the LNN(x) compositions [11] in the complete range $x = 0$–100% show a transition from $NaNbO_3$ to $LiNbO_3$ structural type as a function of increasing Li content, with coexistence of the two phases for intermediate compositions. According to the above-mentioned results, it seems that the complete change from AFE to FE is not exactly fixed for a certain composition, but is rather a gradual change in a composition interval around $x = 2\%$.

All these data indicate that FE and AFE couplings are very close in energy and that small perturbations can induce the change from one to the other quite easily.

Anomalies in the real part of the permittivity (ε') in LNN(0) at 463 K [12, 13] and the thermal behaviour of the Raman modes of LNN(0) [14] suggest the existence of phase transitions around those temperatures. Given the known structural equivalence between poled LNN(0) and KNN(x) with $x = 2.5\%$ K content [5] it becomes interesting to find out the influence of the Li content on the structural heterogeneity of the sodium niobate and the stabilization of a FE phase. In this work we present the study of complex dielectric permittivity, thermal expansion and Raman spectra of LNN(x) compositions with $x \leqslant 5\%$ as a function of the temperature to get information that helps in the understanding of the peculiar structural behaviour of these compounds.

2. Experimental procedure

Ceramics of lithium–sodium substituted niobates LNN(x) of nominal composition $Li_xNa_{(1-x)}NbO_3$, ($0 \leqslant x \leqslant 5\%$) have been prepared by a solid-state chemical reaction at temperatures of 1073 K of stoichiometric mixtures of the component oxides and carbonates.

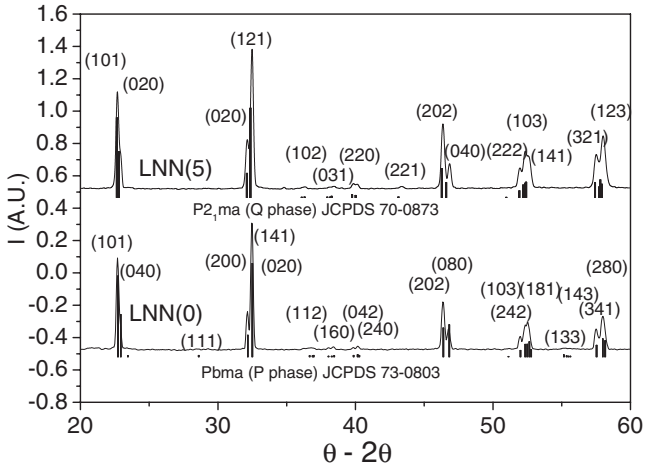

Figure 1. Powder x-ray diffractograms of the LNN(0) and LNN(5) ceramic samples. The reflections for the orthorhombic *Pbcm* phase (P) JCPDS 73-0803 file and orthorhombic $P2_1ma$ (Q) JCPDS 70-0873 file are included as bar diagrams for comparison. The miller index of the main reflections are depicted in the diagrams. For phase P the miller index is given in the *Pbma* setting for better comparison with the Q phase.

Ceramics with 90–93% densification were obtained by sintering pellets in air at 1513 K for 4 h. X-ray diffraction patterns of the thermally annealed ceramics were recorded using a Siemens D-500 with Cu Kα radiation in Bragg–Brentano geometry. The apparent crystallite size was obtained from the full width at medium height (FWMH) applying the Scherrer equation.

Electrodes of 873 K sintered silver paste were used to electrode rectangular samples of $4 \times 7 \times 0.5$ mm^3 dimensions. Dielectric measurements at different frequencies (100 Hz–1 MHz) as a function of the temperature (300–698 K) were performed with a HP4284A LCR Precision meter during the heating–cooling cycle with a rate of 1.5 K min^{-1}. The applied ac voltage was lower than 20 mV cm^{-1}. Thermal expansion measurements (300–698 K) were performed at a temperature rate of 2 K min^{-1} in a Perkin Elmer DMA 7. Raman experiments were recorded in a Dilor XY spectrometer with excitation at 514.5 and 573 nm. The spectral resolution was better than 3 cm^{-1}. A Linkam TP91 unit was used for measurements above RT.

3. Experimental results

The x-ray diagrams for the LNN(0) and LNN(5) are shown in figure 1. The JCPDS files 77-0873 and 73-0803 corresponding to orthorhombic $P2_1ma$ (Q) and *Pbma* (P) phases are included as bar diagrams below the LNN(5) and LNN(0) diagrams, respectively.

The x-ray diffraction diagrams of both samples are quite similar, as expected from the JCPDS files. The LNN(5) sample seems to be closely related to the Q phase, while the LNN(0) sample seems to be more related to a P phase. The LNN(5) diagram shows a shift to larger 2θ indicating a shrinkage of the cell volume as compared with the JCPDS standard. It should be noted that the reported Q phase in the $NaNbO_3$ compound is induced by an electric field. Due to the difference in size between the Na^+ and Li^+ a decrease in cell size in increasing the Li^+ content can be expected. The estimated apparent crystallite size for the LNN(0) sample obtained from the FWMH of the (101) reflection is 73 nm. For the LNN(5) sample this value is

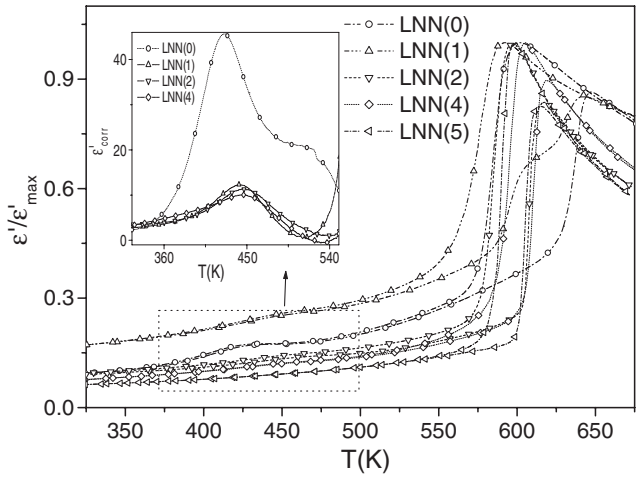

Figure 2. Variation of the normalized $\varepsilon'(T)/\varepsilon_{max}$ for LNN(x) 0(——··○——··), 1(——··△——··), 2(– – –▽– – –), 4(· · · · · ·◇· · · · · ·), 5%(— · —·—— ◁ — · —·——). The data showed the whole thermal cycle. In the inset we show the corrected dielectric constant values $\varepsilon'_{cor}(T)$ values for samples with $x = 0, 1, 2, 4\%$ in the temperature region where the low temperature dielectric anomaly is observed on the cooling run.

58 nm extracted from the equivalent (101) reflection. All the peaks appearing in both diagrams can be indexed in the orthorhombic cell. It can be concluded that, within XRD sensitivity, both samples can be considered as being pure, free of secondary phases and of good enough quality.

3.1. Dielectric properties

Figure 2 shows the normalized dielectric constant ($\varepsilon'/\varepsilon'_{max}$) as a function of the temperature at 500 kHz in a complete heating–cooling cycle for samples with $x = 0\%, 1\%, 2\%, 4\%$ and 5% of Li content. The most intense peak has been attributed to the phase transition from AFE (P) to AFE (R) phases for the $x = 0\%$ sample or to a FE to AFE or PE phase transition for Li substituted samples.

The highest transition temperature is for $x = 0\%$ (647 K, heating run). For $x = 5\%$ the temperature of the dielectric constant maximum T_m drops to 615 K. An interesting result is obtained for $x = 1\%$ where two consecutive anomalies are found at 608 and 642 K, close in temperature to the dielectric maxima of $x = 5\%$ and 0% samples, respectively. The $\varepsilon'(T)$ curves of the $x = 0$–4% Li content samples also show a wide, small maximum in the 425–460 K range showing a slight thermal hysteresis. Sample LNN(5) only presents a FE–(AFE/PE) phase transition peak.

To better analyse the $\varepsilon'(T)$ small wide maxima, the values corresponding to a regular FE or AFE transition behaviour, $\varepsilon'_{FE/AFE}(T)$, should be subtracted from the experimental $\varepsilon'(T)$ curves. The procedure to obtain $\varepsilon'_{FE/AFE}(T)$ was as follows. From the $1/\varepsilon'(T)$ curve for the highest measurement frequency (1 MHz), figure 3, the values corresponding to the linear part that follows the Curie–Weiss-like law below the phase transition temperature were obtained, fitted and extrapolated to lower temperatures (dashed line in figure 3). Fixing the slope and slightly varying the ordinate at the origin the other linear fits at lower frequencies are obtained. Once $\varepsilon'_{FE/AFE}(T)$ values at each frequency were obtained, they were subtracted from the experimental values yielding the corrected dielectric constant values, $\varepsilon'_{cor}(T) =$

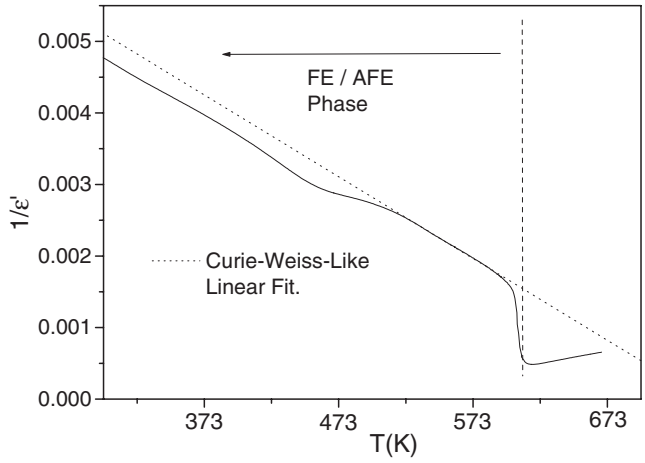

Figure 3. Variation with temperature of the reciprocal of the dielectric constant at 1 MHz for sample LNN(2). The dotted straight line is the extrapolation of the linear region (Curie–Weiss-like behaviour) in the curve. This straight line represents the dielectric constant variation in the ferroelectric/antiferroelectric phase below the main phase transition temperature.

Table 1. Temperatures of the dielectric and thermal expansion anomalies.

	Main dielectric anomaly (K)		Small dielectric anomaly (K)[b]		Thermal expansion anomaly	
Li content (%)	*Heating*	Cooling	*Heating*	Cooling	*Heating*	Cooling
0	*647*	601	*425*	429	*648*	595
1	*608/642*[a]	592	*445*	441	*602/636*[a]	584
2	*617*	597	*456*	448	—	—
4	*619*	605	*452*	445	—	—
5	*615*	600	—	—	*622*	605

[a] The LNN(1) presents two main dielectric and thermal expansion anomalies in heating.
[b] The values are obtained at 300 kHz.

$\varepsilon'(T) - \varepsilon'_{\mathrm{FE/AFE}}(T)$. The inset in figure 2 shows $\varepsilon'_{\mathrm{cor}}(T)$ for the samples $x = 0, 1, 2, 4\%$ measured at 500 kHz on cooling. The observed anomaly is larger for the $x = 0$ sample, the dielectric constant at maximum decreases strongly with the Li addition even for doping as low as 1% and disappears for $x = 5\%$. The temperature at the maximum of the anomaly, in the cooling run, increases from 425 K at $x = 0\%$ to 450 K at $x = 4\%$ (see inset in figure 2). The diffusivity of the observed anomaly also increases with the increase of Li doping. The temperatures of the dielectric anomalies are gathered in table 1.

In order to extract information about the nature of the observed anomaly, the corrected real part of the dielectric permittivity and the as measured dielectric loss, $\varepsilon''(T)$, as a function of the temperature at different measuring frequencies for samples with $x = 0$, 2% Li in the heating run are shown in figure 4. The $x = 2\%$ composition has been taken as representative of the $x = 1\%$–4% Li content range.

The plot of figure 4(a) shows the maxima around 429 K of the curves for the LNN(0) sample as a function of the temperature for different measurement frequencies. The dispersion with frequency of these maxima is negligible. It should also be noted the presence of another more diffuse maximum around 558 K that is not clearly observed in the raw dielectric data. The

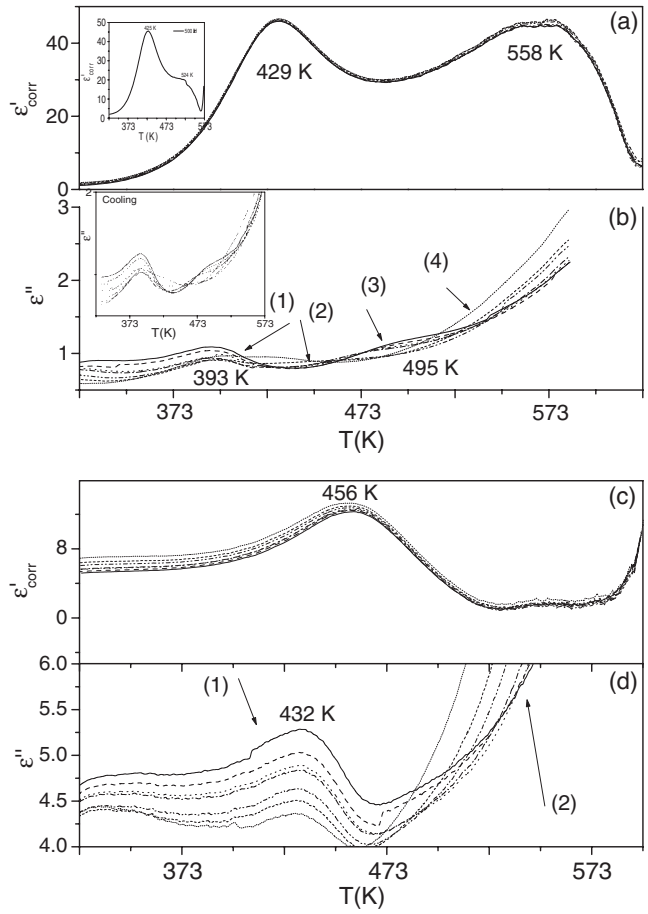

Figure 4. (a) $\varepsilon'_{\rm corr}(T)$ at different frequencies (100 kHz (——), 200 kHz (– – –), 300 kHz (——··), 500 kHz (— · —), 600 kHz (· · · · · ·), 800 kHz (– – –), 1 MHz (——)) for sample LNN(0), heating run. The different measuring frequencies and the temperatures at maximum are depicted in the plot. (b) $\varepsilon''(T)$ for sample LNN(0), at the same frequencies, heating run. The temperature at the maximum for the highest frequency is depicted. The numbers represent regions where the dielectric loss behaviour with increasing measuring frequency is different. The inset is the same plot but in the cooling run, showing the good reversibility of the observed anomalies. (c) $\varepsilon'_{\rm corr}(T)$ at different frequencies (100 kHz (——), 200 kHz (– – –), 300 kHz (—— · ·), 500 kHz (— · —), 600 kHz (· · · · · ·), 800 kHz (– – –), 1 MHz (——)) for sample LNN(2), heating run. The different measuring frequencies values and the temperatures at maximum are depicted in the plot. (d) $\varepsilon''(T)$ for sample LNN(2), at the same frequencies, heating run. The temperature at maximum for the highest frequency is depicted. The numbers represent regions where the dielectric loss behaviour with increasing measuring frequency is different.

corrected response shows small dispersion and no change of the maximum position at different frequencies can be observed. The shape, intensity and position of this anomaly are difficult to determine because it is close to the main dielectric anomaly and so it is much affected by the correction procedure. In the plot of the imaginary part $\varepsilon''(T)$, figure 4(b), it was possible to distinguish four different regions depending on the increase or decrease of the dielectric losses with increasing frequency. Region 1 showed an increase of the losses on increasing the measuring frequency but no change in the maxima position (393 K). The position of the

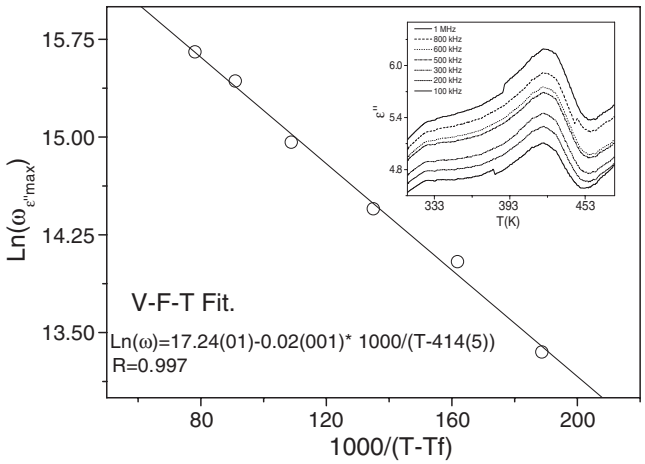

Figure 5. Logarithm of the frequency of the dielectric loss maximum as a function of the reciprocal of the temperature after the Volger–Fulcher–Tamman law for sample LNN(2) in the cooling run. The inset shows the dielectric loss from which the temperature at maximum at each frequency were collected.

maximum of the dielectric losses in region 1 is around 36 K less than that of the dielectric constant maximum T_m. In region 2 the dielectric losses decrease with increasing the measuring frequency and a small maximum is observed at the lowest frequency. In region 3 again the dielectric losses increase with the measuring frequency with a maximum around 495 K that changes its position with the frequency mainly due to the strong increase in the losses produced in region 4 where again the dielectric losses are larger for lower frequencies. The results on cooling showed a small hysteresis of the lower temperature maxima (around 4 K less). The second anomaly presents larger hysteresis (≈37 K) and a lowering in its dielectric constant values. On cooling the dielectric loss shows small hysteresis, see inset in figure 4(b).

The dielectric response of the LNN(2) sample is different, figure 4(c). The $\varepsilon'_{corr}(T)$ curves are more dispersive, there is a reduction of the dielectric constant dispersion with the measuring frequency for temperatures larger than T_m (456 K) and the T_m increases when the measuring frequency increases. The second maximum clearly observed in LNN(0) is strongly reduced, and its possible position is around 551 K. The as measured $\varepsilon''(T)$ behaviour of the LNN(2) sample is simpler than the one obtained for LNN(0), figure 4(d). Just two regions of different behaviour were identified. In region 1 (see figure 4(d)) the losses increase with increasing frequency. The temperatures of the maxima are lower than those of $\varepsilon'_{cor}(T)$ maxima (≈24 K) and they increase in value and temperature with increasing measuring frequency. In region 2 the losses are larger for lower frequencies and no maxima was observed. Larger hysteresis is found between the heating and cooling runs (6 K) for the low temperature maxima in comparison with LNN(0). This behaviour and the remarkable decrease of $\varepsilon''(T)$ above the temperature of the maxima are typical of relaxor-like phase transitions.

In figure 5 we have plotted the natural logarithm of measuring frequency as a function of the corresponding reciprocal of the temperature at maximum of dielectric losses (inset of figure 5) in the cooling run for the LNN(2) sample according to the Vogel–Fulcher–Tamman law:

$$Ln\omega_{max} = Ln\omega_0 - E_a/k(T_m - T_f), \tag{1}$$

where ω_{max} is the measuring frequency, T_m is the temperature at the maximum of $\varepsilon''(T)$

at that frequency, ω_0 is the attempt frequency, E_a is an activation energy, and T_f the freezing temperature. The increase in the losses due to conductivity in the low frequency range prevents defining the maxima of $\varepsilon''(T)$ below 100 kHz reliably enough to take a good value of their temperature, therefore we have used only one decade of frequency (0.1–1.0 MHz) in the analysis of the relaxor-like behaviour shown in figure 5.

The main plot fits rather well to a smooth Vogel–Fulcher–Tamman law with a freezing temperature T_f of 414 K $E_a = 2$ meV and a ω_0 close to 3×10^7 rad s^{-1}. Similar values of both the activation energy and the relaxation frequency have been reported for example in the impurity-induced ferroelectric relaxor-like behaviour in $SrTiO_3$ and $BaTiO_3$ [15]. It should be noted that using the temperatures at maxima at different frequencies from the $\varepsilon'_{cor}(T)$ curves the parameters obtained for the Vogel–Fulcher–Tamman law are very similar.

The dielectric response of the LNN(5) shows only one anomaly at 615 K on heating with a thermal hysteresis of 15 K. The wide maximum at 456 K has disappeared which indicates that the origin of the relaxor-like behaviour is not maintained. This sample presents the lowest dispersion of the dielectric constant with frequency and no other anomaly is observed.

3.2. Thermal expansion

Thermal expansion measurements on samples with $x = 0\%, 1\%$ and 5% Li content have delivered the results that are shown in figures 6(a), (b), where the thermal expansion curves (a) and their derivatives (b) are plotted. The curve for the sample with $x = 0\%$ shows a small negative jump at 648 K (the negative peak of the derivative, figure 6(b), clearly confirms the sign of the jump) corresponding to the (AFE)P–(AFE)R phase transition. The expansion behaviour of the sample in the temperature range below the main transition showed different fluctuations. As can be seen in the derivative curve the sample has thermal expansion coefficient fluctuations below 500 K with an increase in the coefficient at around 400 K and then a decrease close to 500 K. On cooling, the main minimum has strong hysteresis as found in the dielectric measurements (51 K). The thermal expansion curve for LNN(1) is similar to that of sample LNN(0), there are no strong changes in the curve, reflecting small volume changes. Two well-defined minima are present in the derivative curve (figure 6(b)), one at 602 K and the other at 636 K. Slight dimensional changes are observed at the temperatures of the derivative peaks. The minimum at higher temperature is stronger than for LNN(0) and appears at lower temperatures. In the cooling only one well-defined minimum is observed at 584 K. The thermal expansion coefficient behaviour agrees rather well with the dielectric constant one (figure 2). The derivative curve of this sample presents thermal expansion coefficient fluctuations below 500 K as the LNN(0) does, figure 6(b), but with lower intensity.

Concerning the sample with $x = 5\%$ Li the thermal expansion curve presents a strong negative jump reflecting strong volume changes in the sample at 622 K with significant thermal hysteresis. In the derivative curve a large minimum is observed at 622 K in heating that is quite close to the temperature of the dielectric constant maximum (615 K), corresponding to the main phase transition. It is interesting to note that this sample did not show any fluctuation in the thermal expansion coefficient apart from the main phase transition.

3.3. Raman study

In order to complement the data on the anomaly found at about 425–460 K, Raman experiments on the $x = 0, 1\%$ and 5% samples from RT to 800 K were performed. Figure 7(a) shows the Raman spectra of LNN(0) to LNN(5) from 40 to 500 cm^{-1} (the inset shows the higher frequency bands). The spectra at RT show similar features as those appearing in previous works [11, 16].

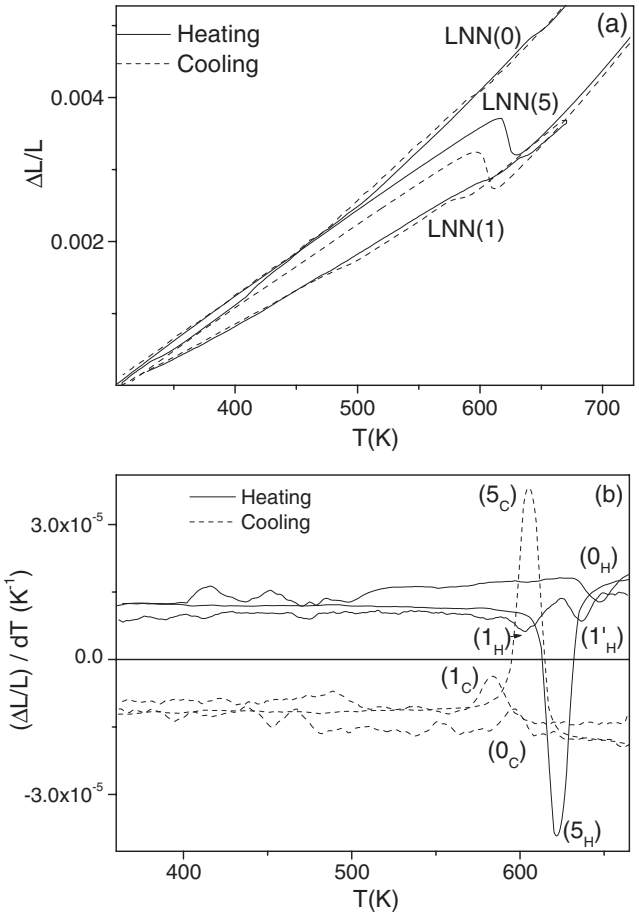

Figure 6. (a) Thermal expansion curves in the whole temperature cycle for samples with lithium content $x = 0, 1, 5\%$. Heating: continuous curve, cooling: dashed curve. (b) Thermal expansion coefficient in the whole temperature cycle for samples with lithium content $x = 0, 1, 5\%$. Heating: continuous curve, cooling: dashed curve.

Compositional [11] studies of the Raman spectrum of LNN(x) showed that three peaks appear in the 50–100 cm^{-1} frequency interval for $x = 0$ and only a single peak for compositions with $x > 5\%$. These bands have soft mode character and have been attributed either to Na^+ vibration [9, 16] or to a Nb–O_6 octahedra tilt [17]. It is surprising that no-one has yet attributed them to Nb vibrations, which would completely explain the experimental results of soft-mode behaviour from polar to non-polar phases, low frequency and similarity with other Nb perovskites such as $AgNbO_3$ [18], $KNbO_3$ [19] and $La_{1/3}NbO_3$ [20].

The relevant result for this work is that the presence of a multiple or single peak in that region is associated with the AFE or FE character of the samples, respectively. In our case, a single band is already found in some spectra of $x = 1\%$. The bands at 124 and 156 cm^{-1} are also seen to decrease with increasing lithium content, as shown in figure 7(a). It should be noted that the band at 124 cm^{-1} is not present in certain regions of the LNN(1) sample (see figure 8) and not at all in the LNN(5) sample. On the contrary a high frequency band at $\nu \approx 870$ cm^{-1} is seen to increase with increasing lithium content (see also [11] for spectra of samples with higher x). The origin and relevance of this band will be discussed later.

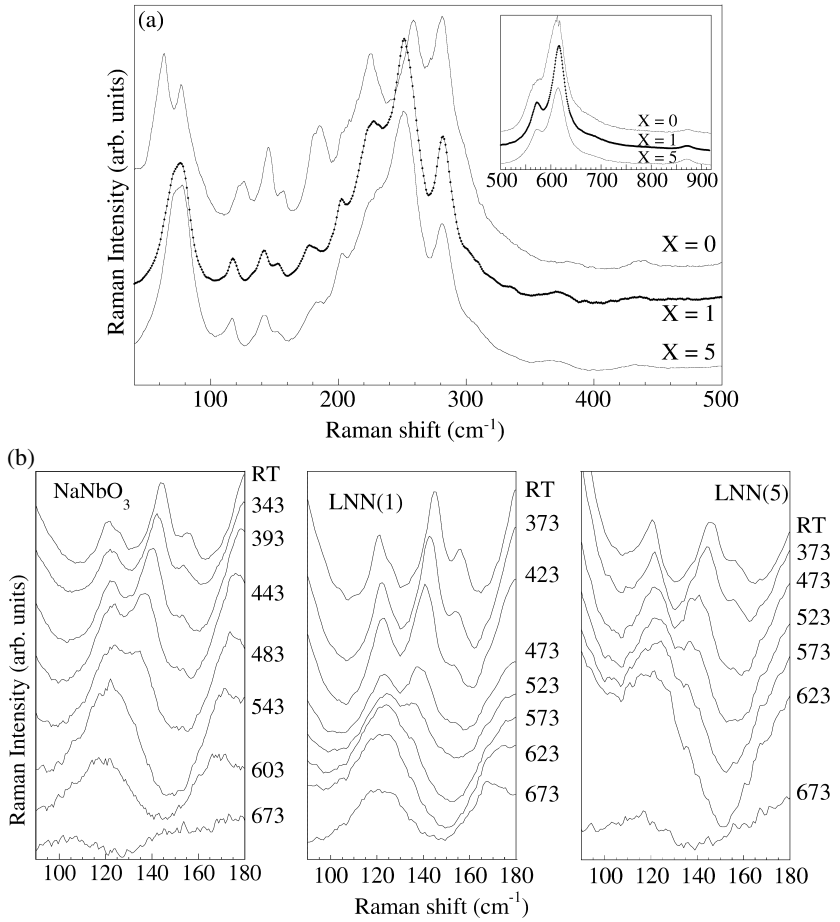

Figure 7. (a) Room temperature Raman spectra of LNN(x) samples for $x = 0$, 1 and 5% Li content on the low frequency side. The inset is the high frequency part of the spectrum of the same samples. (b) Temperature evolution of the Raman spectra of LNN(x) samples for $x = 0$, 1, 5% in the 90–180 cm^{-1} range.

Figure 7(b) shows the 90–180 cm^{-1} region of the spectrum of LNN(0), LNN(1) and LNN(5) as a function of increasing temperature. This region is especially interesting since bands appearing in it have been assigned to NbO_6 octahedra tilts [16] that are relevant in many phase transitions in perovskites.

In this temperature range some bands change noticeably their frequencies or intensities. First, the weak band at 124 cm^{-1} (when present) disappears at a temperature around 420 K. From RT to 500 K the 120 cm^{-1} band hardens while the 145 cm^{-1} band softens. They have fully coalesced at a temperature between 520 and 620 K that increases with x. Simultaneously the 156 cm^{-1} band decreases gradually and disappears at about 470 K. These features are common to all three samples, except for the disappearance of the 124 cm^{-1} band, which is absent in the $x = 5\%$ composition.

We can derive more information about the structural change taking place at this temperature from the spectra shown in figure 8, where we present the 50–180 cm^{-1} region of $x = 0$ and 1% samples taken in different points. The inset of this figure shows the high frequency bands

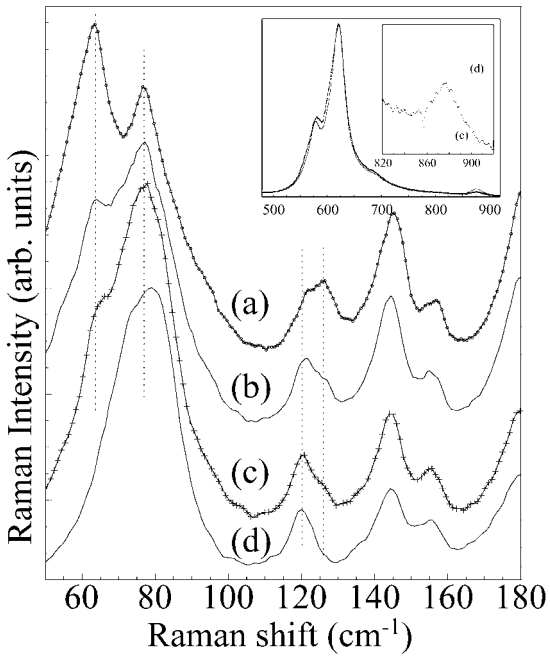

Figure 8. Raman spectra of LNN(0) ((a), (b)) and LNN(1) ((c), (d)) recorded in two different points of each sample. The inset shows the high frequency region of spectra (c) and (d).

corresponding to the two spectra of LNN(1). From the relative intensities of the two peaks in the 50–90 cm^{-1} region we attribute spectra (a) and (b) of $NaNbO_3$ to regions with more or less P character, respectively, reflecting the heterogeneous nature of the compound. Both spectra can be interpreted either as a superposition of those pertaining to P and Q phases, with different proportions, or from phases intermediate between P and Q, being (a) and (b) closer to P and Q spectra, respectively. Correspondingly, spectra (c) and (d) are attributed to regions of LNN(1) with more or less AFE phase content, respectively, suggesting that a ferroelectric Q-like phase can also co-exist with the AFE P phase in this composition.

4. Discussion

4.1. LNN(0) compound

The dielectric constant variation with temperature showed the anomaly characteristic of a first order phase transition with a significant thermal hysteresis corresponding to the AFE (P)–AFE (R) phase transition. Two more anomalies are observed, at 425 and 558 K, after the correction of the main contribution to the dielectric constant. The two small maxima found in the dielectric constant are related to two maxima in the dielectric loss that showed an increase in the loss value with the increase in measuring frequency (regions 1 and 3 in figure 3(b)). The region between them (2) and for larger temperatures (4) showed regular FE/AFE behaviour with increasing temperature (larger losses in decreasing measuring frequency). The observed behaviour in regions 1 and 3 are close to that observed in relaxor ferroelectrics with the exception that in this case the relaxor dispersion that produces the change in the maximal position is not observed, probably because the temperature shift is smaller than the accuracy of our experiment.

The structural complexity of $NaNbO_3$ has been known for a long time. As explained in the introduction, the coexistence of two phases, AFE (P) and FE (Q), is possible for this composition. Lefkowitz *et al* [21], studying single crystals of $NaNbO_3$, pointed out that the existence of both phases depends on the particular single-crystal studied and also on its size. Phase Q was only found in large crystals. They also postulate that free energies of the P and Q phases cross each other at two temperatures, the Q phase being stable for temperatures in the approximate range (393–533 K). On the other hand Chen and Feng [4] by TEM studies demonstrated the relationship between the existence of phases P and Q and the variations in Na^+ stoichiometry in the crystals. According to these authors, phase Q is related to Na^+ rich regions and phase P to Na^+ poor ones. They also reported that the mixture of phases P and Q was in the domain scale. Reznichenko *et al* [22] postulated that the existence of P and Q phases in $NaNbO_3$ is related to the production of anionic vacancies in the initial Nb_2O_5 reagent due to the instability of the valence state (4^+, 5^+) of Nb.

The crystal structure of the antiferroelectric P phase belongs to the orthorhombic $Pbma$ space group with the cell quadrupled in the b axis with respect to the ideal perovskite cell $b = 4a_c$ [23]. Phase Q belongs to the orthorhombic $P2_1ma$ space group and the cell is doubled in the b axis [23], $b = 2a_c$. The main structural differences arise from the way in which successive layers of octahedra are arranged along the [010] axis. In-phase and out-of-phase tilts (b^+ and b^- in Glazer notation) alternate every two-perovskite layers in the P phase while only in-phase tilts remain in the Q-phase. In parallel to this, Nb displacements change from an intermediate between one- and two-corner shift in the P phase to an exact two-corner shift in the Q-phase. Moreover, Nb couplings along the b axis are AFE in the P phase and FE in the Q phase. These changes also affect the coordination polyhedra around Na^+.

The Raman spectra measured in different points of a LNN(0) ceramic (curves (a) and (b) in figure 8) showed the presence of the double peak in the 50–90 cm^{-1} region with varying intensities. As previously explained, spectrum (a) is attributed to regions with predominant AFE (P) character, while spectrum (b) is assumed to be intermediate between those corresponding to pure AFE (P) and FE (Q) phases, suggesting that AFE and FE regions coexist in $NaNbO_3$.

Variations in the relative intensities of the bands at 120–124 cm^{-1} are correlated with variations in the intensities of the double peak in the 50–90 cm^{-1} region. The 124 cm^{-1} band decreases when the 63 cm^{-1} band does. Other unresolved splittings with similar behaviour are observed at higher frequencies (180–185, 252–258 cm^{-1}, etc).

Bands appearing in the spectral region from 100 to 180 cm^{-1} have been attributed to vibrational tilts (or librations) of NbO_6 octahedra [16]. Since the main difference between P and Q phases, as regards octahedra tilts, is the presence of both in-phase and out-of-phase (b^-, b^+) tilts in the P phase, with only in-phase tilts in the Q phase, we may attribute the 120–124 doublet to in- and out-of-phase vibrational tilts around the b axis, respectively. Then, the reduction in the intensity of the 124 cm^{-1} band is related to the loss of the anti-phase tilt in the Q phase. The other two peaks at about 145 and 156 cm^{-1}, which are present both in P and Q phases, should be attributed to tilts around the a and c axes (in any order). These results support the large structural heterogeneity of the LNN(0) composition.

Within this interpretation, the disappearance of the 124 cm^{-1} band on increasing temperature implies that the b^- tilt becomes inactive, and that the structure evolves towards another one containing only b^+ tilts, such as the Q phase.

The behaviour of the thermal expansion of this sample shows a small dimensional change in the P to R phase transition with strong thermal hysteresis. The derivative curve in heating showed fluctuations below 520 K whose directions (signs) could reflect the sequence of phase transitions that leads to the dielectric constant anomalies at 429 and 558 K. It is interesting

to emphasize the smallness (even in the main phase transition temperature, 649 K) of the dimensional jumps. The phase transition at 649 K produces a slight volume reduction.

From these considerations it is possible to infer the possible origin of the observed dielectric anomalies below the main AFE/AFE dielectric maximum. Due to the known structural heterogeneity of $NaNbO_3$, in the prepared ceramics there are some minority regions of the Q phase in a majority but inhomogeneous P phase. On increasing the temperature some of the P regions undergo a phase transition to a Q phase due to the change in free energy producing the stabilization of the Q phase (first anomaly, at about 429 K). From the structural point of view, a loss of anti-phase tilts around the orthorhombic *b* axis takes place, and this is accompanied by a reorientation of Nb cations from AFE to FE ordering. The Q phase produced is stable only in a narrow temperature range and at about 558 K returns to another phase, probably similar to the P phase, that evolves at a higher temperature to the R phase. Whether the phase formed after the second anomaly is AFE, P-like or a new FE phase cannot be definitely established from our experiments. The evolution of the Raman spectra at these temperatures, in any case, suggests that the second anomaly also involves changes in octahedra tilting.

On cooling, the large hysteresis observed in the main dielectric anomaly prevents us from seeing the second anomaly in the real part of the permittivity with enough accuracy, but the dielectric loss showed good reversibility of the process with the same sequence of phases in the reverse direction. The good reversibility of the first anomaly and that of the dielectric losses supports the assumption that there is a small amount of Q phase initially present in the $NaNbO_3$, because, as pointed out in [22], single crystals of $NaNbO_3$ with a certain initial ratio of Q phase did not change this ratio by thermal treatment, while crystals without Q phase presented, on cooling, a P and Q phase mixture. Cheng and Feng [4] postulated independent phase transitions paths for P and Q phases in $NaNbO_3$. In the temperature interval of this study, the authors [4] established that P phase changes to R1 at 653 K and phase Q changes to Q1 at 553 K and Q1 to Q2 at 723 K. We note that the Q–Q1 transition temperature is coincident with the temperature of the second anomaly observed in our data. Nevertheless, our experimental results are in better agreement with the work of [21] and [22], where phase Q reverts to phase P on increasing temperature. The small values of the dielectric constant in the anomalies, the small thermal hysteresis and the behaviour of the dielectric losses indicate that the phase transition is produced in small volumes, not in the entire sample.

The P $\rightarrow$ Q transition involves changes in the sense of tilting of the octahedra and in the Nb displacement. This represents a major organization of the structure that should imply a large energy barrier [24]. However, the transition may be helped by the dynamical relaxation of Nb ions among equivalent off-centre sites, recently proposed in the interpretation of low-frequency Raman spectra [17]. The reversibility of the process indicates that it takes place in the same regions in the heating and cooling runs. This is as expected since the structural heterogeneity is fixed during the ceramic preparation and cannot be changed in the temperature interval of this study. Thus the sample preparation method used in this work produces $NaNbO_3$ ceramics where the P and Q phases are energetically close and some P regions can be easily converted to the Q phase.

4.2. Li addition

The temperature and hysteresis of the main dielectric anomaly decrease for Li containing compounds. The addition of Li also affects the small anomalies producing the gradual decrease of the first one (between 429 and 460 K) with lithium content increasing from 0 to 4% and the near disappearance of the second small one (around 550 K) for $x = 2\%$. The lack of frequency dispersion and other anomalies apart from the main FE $\rightarrow$ (PE/AFE) phase

transition in sample LNN(5) supports considering this sample as a single ferroelectric phase. It should be noted that the dielectric response of LNN(1) seems to be in an intermediate stage between the dielectric responses of LNN(0) and LNN(5) phases, presenting two maxima of the dielectric constant in the heating run at temperatures close to those of LNN(0) and LNN(5) (see table 1), respectively, and also keeping the low temperature small wide anomaly. The total relaxor dispersive behaviour is slightly observable in LNN(1) and clearly observed for 2% and 4%, as was demonstrated for the anomaly at 456 K of the LNN(2) sample, figures 4(c), (d). This behaviour can be related to the critical concentration of Li that is needed to induce ferroelectric character in the sodium niobate. From our results the critical concentration of Li to produce the phase change should be in the interval $1\% < x_c < 2\%$. This result is in agreement with the piezoelectric results of Zeyfang *et al* [25] where the the start of the measurable planar coupling coefficient in Li^+ modified $NaNbO_3$ was at about 1.5% Li.

The thermal expansion results for sample LNN(5) indicate that this composition suffers a single phase transition with important dimensional and structural changes. The character of this transition is unclear but the strong dimensional changes found support a possible FE/PE phase transition. The work of Nitta [26] on the properties of sodium lithium niobates showed a decrease in the temperature gap between the ferroelectric and paraelectric phase transition for a Li content between 4 and 6%. The first paraelectric phase on heating in the $NaNbO_3$ phase diagram is the orthorhombic S phase. It is possible that for a Li content of 5% the phase transition is ferroelectric Q-like to a paraelectric S phase. The mechanoelastic properties of this sample, [3], also support this assumption because the LNN(5) sample showed just three high temperature phase transitions instead of the four present in $NaNbO_3$ as obtained from different techniques.

As regards the LNN(1) composition, figure 6 shows that the temperature of the main dimensional (structural) change (about 602 K) does not coincide with that of the largest peak of the dielectric constant at 642 K, where only slight dimensional changes are observed. On the contrary, it is closer to the dielectric peak at 615 K and also to the temperature of the thermal jump in LNN(5), 622 K (see table 1). The LNN(1) composition contains a rather high starting proportion of Q-like phase that suffers, as in LNN(5), a phase transition with important dimensional changes, suggesting the transformation to a paraelectric phase. The remaining P phase volume maintains the transition scheme close to that obtained for LNN(0), with a $P \rightarrow R$ transition at 637 K (thermal expansion data) or 642 K (dielectric data). In this sample the remaining P phase is the minority one and so the dimensional changes related to the P–R transition are weakly observed (figure 6(a)). As LNN(0), the LNN(1) sample presents a strong structural heterogeneity.

The Raman curves (c) and (d) in figure 8 show qualitatively the same result as LNN(0). The relative intensity of the bands in the 50–90 and 120–124 cm^{-1} regions indicate that in this case the Q-like FE phase is the majority one. As shown in figure 7, in the Raman spectrum of LNN(5) the bands at 63 and 124 cm^{-1} have completely disappeared, in agreement with the increasing tendency to Q-phase stabilization upon lithium doping. A decrease in the intensity of the 156 cm^{-1} band is also observed.

Some more information concerning P and Q phases can be drawn from the high frequency bands shown in the inset of figure 8. The 870 cm^{-1} band has always been neglected in the discussion of Raman spectra since ν_1 and ν_2 modes of Nb–O_6 octahedra, corresponding to high frequency Nb–O stretching vibrations, can be identified with the 580 and 600 cm^{-1} components of the broad intense band [11]. The high energy of the 870 cm^{-1} band as well as comparison with spectra of many other Nb oxides [19] allows us to propose that it arises from shorter (named terminal) Nb–O bonds that are caused, in general, by some perturbation close to the Nb–O_6 octahedron. In LNN(x) compounds this perturbation may be the absence of a

sodium cation, the associated oxygen vacancy, or, in lithium-containing samples, the proximity of a Li^+ cation.

Within this interpretation, the difference observed between spectra (c) and (d) of the inset, both corresponding to 1% lithium content but with different degree of coexistence of P and Q-like phases, clearly indicates that different octahedra distortions are involved in these two phases. In particular, octahedra seem to be more distorted in Q-like regions, suggesting (contrary to the hypothesis given by Chen and Feng, [4]) that the P phase is formed in Na stoichiometric regions.

As commented on in the introduction, another ferroelectric phase, different from the Q phase, has been found at room temperature in $Li_xNa_{1-x}NbO_3$ single crystals for $x = 2$ and 3% compositions [8, 10]. We hereafter refer to this phase as phase L. This ferroelectric phase was orthorhombic with $Pc2_1b$ space group. The cell keeps the $b = 4a_c$ parameter, but has lower symmetry than the P phase. As regards octahedral tilts, the only difference is that the alternance of in-phase and out-of-phase tilts along the b axis is changed. This yields differences in the alkaline cation environment, except that phases P and L are very close. The ferroelectricity in phase L does not come from the Nb displacements but from relative displacements of the ensemble of negative ions with respect to the positive ones [10]. As commented on before, there are small differences among the powder x-ray diagrams of the P, Q, and the L phases. For phases P and L the diagram is practically the same. For the Q phase there are slight differences, the largest ones being the absence of the peak corresponding to (133) reflection, P phase indexing, (55.3° 2θ) and of any reflections (111) (131) between the (101)(040) and (020)(141)(002) main diffraction peaks in the $NaNbO_3$ diagram at room temperature. The powder x-ray diffraction of the LNN(5) sample does not present any peak at those positions. The diagram seems to be simpler and closer to that corresponding to the Q phase than to that of the L phase which should keep the (133) reflection at 55.3 2θ as well as the (131) reflection at 28.7° 2θ. As regards Raman scattering, the similarity of P and L structures suggests that their spectra should not be very different, contrary to the experimental finding that the spectrum of doped samples differs considerably from that of undoped $NaNbO_3$. Specifically, the differences observed in the low frequency modes, here assigned to Nb vibrations, between the spectrum of the P phase of LNN(0) and that of Li-doped samples suggest that the latter should be associated with a phase with substantially different Nb displacements as compared with the P phase. A Q-like phase fulfils this requirement. In view of these results it is likely that all Raman spectra reported in the literature for Li-doped ceramics should be interpreted as belonging to a Q-like phase, and not to the L one.

Moreover, for the LNN(5) composition there is a parallelism between the absence in the Raman spectrum of the peak associated to antiphase tilting b with the disappearance of the dielectric anomaly at about 460 K.

The small intensity of some of the supercell ($\mathbf{b}_{\text{orthorhombic}} = 4\mathbf{a}_{\text{cubic}}$) peaks in the diffraction pattern of LNN(0) shown in figure 1, makes it closer to that of LNN(5) ($\mathbf{b}_{\text{orthorhombic}} = 2\mathbf{a}_{\text{cubic}}$). As the LNN(0) sample is in a majority AFE P phase and the LNN(5) seems to be in a stable Q-like phase, the small changes in the x-ray diagram can be related to a smaller magnitude of the out-of phase tilt in our LNN(0) samples, and so the evolution to an in-phase tilt should be easier. Further work in the structural refinement of these samples is necessary to assess this idea. As a comparison, in the work of Lima *et al* [27] an x-ray diagram of a $NaNbO_3$ ceramic is presented with the corresponding Rietveld fit in the orthorhombic $Pbcm$ space group. This diagram presents all the corresponding supercell lines and the (133) peak at 55.5° 2θ is clearly observed. The apparent crystallite size obtained for this sample was reported to be 60 nm in powder form, close to the value of 73 nm obtained in the LNN(0) ceramic sample in this work. We can say that both samples are of similar quality. The $NaNbO_3$ ceramic sample of [27] is

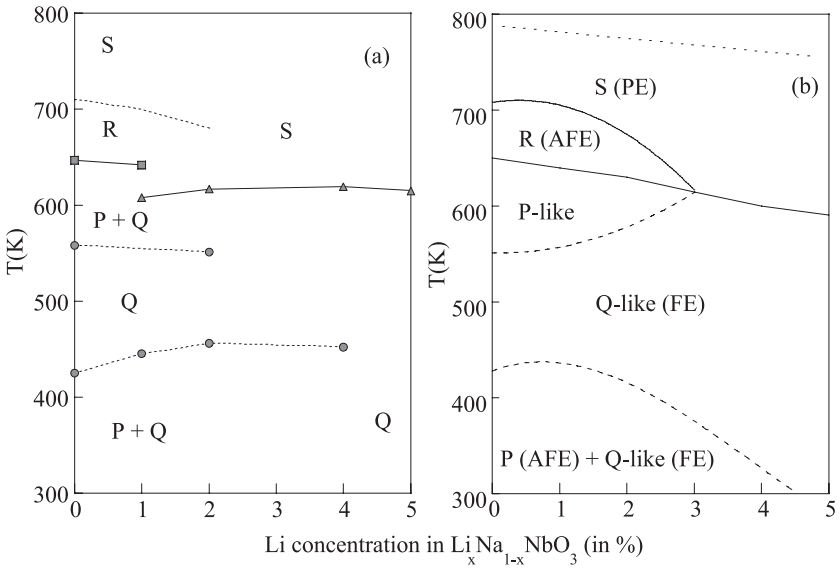

Figure 9. (a) Phase transition temperatures obtained from dielectric and thermal expansion anomalies in this work as a function of the Li^+ content x. (b) Tentative phase diagram in the low Li content side of $Li_xNa_{1-x}NbO_3$ solid solution.

the same as that measured in [6] which did not show the dielectric anomalies discussed in this work. It should be noted that the $NaNbO_3$ ceramic in [6] was prepared by a solution method instead of the classical solid-state reaction used in this work.

For increasing Li^+ doping the Q phase seems to be stabilized and the minority P phase regions are reduced in size, producing a clear relaxor-like behaviour in the transition (first dielectric anomaly). The reversibility of the process indicates, as in the case of the LNN(0) sample, that the occurrence of the minority Q phase is fixed in the sample preparation and the same regions that undergo the P to Q-like transformation on heating revert to the P phase on cooling. The addition of larger quantities of Li^+ doping produces the stabilization of a ferroelectric Q-like phase and the decrease of the presence of the P phase in the samples. In LNN(2) samples the relaxor-like behaviour of the small dielectric anomaly can be related to the presence of a nanostructured antiferroelectric P phase competing in a majority ferroelectric Q-like phase that can produce nanoregions with dipolar-glass behaviour [28]. These small regions undergo a reversible P to Q phase transition. For $x = 5\%$ the sample is homogeneous ferroelectric with a Q-like structure. Recently Yuzyuk *et al* [29] has reported the stability of the Q phase for Li contents larger than 3% with a region of coexistence of P and Q phase between $2\% \leqslant x \leqslant 3\%$, based on structural refinements of synchrotron x-ray diffraction data and Raman scattering. The authors did not report the existence of phase L in their samples. In this work the samples were prepared by solid-state reaction of the corresponding oxides and carbonates.

From the ensemble of data presented in this work we can draw a tentative phase diagram for LNN(x) compounds with $x \leqslant 5\%$, as shown in figure 9. Dashed lines represent the anomalies related to P–Q and Q–P transitions. Due to the structural inhomogeneity, the transition temperatures can vary greatly for samples of nominally the same composition, or even be absent. Therefore, this diagram is only qualitative. Our tentative phase diagram is somehow similar to the phase diagram proposed by Raevskii *et al* [30] for $Na_{1-x}Li_xNbO_3$

single crystals. In this work the Q phase is the stable one for $x > 1\%$ but changes to the P phase at $T > 473$ K or higher for increasing x. For $x = 6\%$ the Q phase does not revert to the P phase. In this phase diagram phase Q evolves to the anti-ferroelectric phase R at around 600 K. Our thermal expansion results for the LNN(5) sample indicate a main structural change at 622 K that is typical of ferro–paraelectric phase transitions. So a Q $\rightarrow$ S phase transition is included in the tentative phase diagram instead of Q $\rightarrow$ R as proposed in [30]. On the other hand no L phase was reported in this work in agreement with our results. Also the authors comment on the strong influence of the solid solution preparation conditions on the phase diagram for low Li content.

The combination of dielectric, thermal expansion and Raman spectroscopy results performed in this work help in the establishment of the compositional regions of the solid solution where the structure presents some degree of instability.

5. Conclusions

All the results presented in this work strongly suggest that the small anomalies found out in the dielectric constant and Raman spectra of the studied compounds at about 450 K are a consequence of the structural heterogeneity of the crystalline grains, which is well known in the case of $NaNbO_3$ single-crystals. This heterogeneity produces regions with different physical properties. Our experimental results permit us to understand the structural evolution of the existing phases in pure sodium and lithium-doped compounds.

For the LNN(0) samples there are regions of the P phase that undergo a phase transition to a Q phase that is not stable into the majority P phase. At higher temperatures the regions of the Q phase revert to the P AFE phase.

Li^+ doping produces the beginning of the stabilization of a Q-like FE phase. Upon increasing the Li^+ content, the larger ferroelectric phase stability makes the remaining regions of the AFE P phase in a majority Q-like phase undergo a phase transition to the Q-like phase producing a structurally homogeneous ferroelectric. This happens for Li content larger than a critical concentration that can be established in the range $1 \leqslant x_c \leqslant 2\%$. For $x = 5\%$ Li only the ferroelectric Q-like phase is present at room temperature.

The relaxor-like behaviour in the Li doping range $2\% \leqslant x \leqslant 4\%$, could be attributed to the existence of the transition of a nanostructured AFE P minority phase to a majority FE Q-like phase that can produce nanoregions with a dipolar-glass behaviour in a certain temperature interval. These regions are fixed in the preparation procedure where the structural heterogeneity is produced.

The origin of the structural heterogeneity cannot be inferred from our results.

Acknowledgments

This work has been supported by LEAF Project G5RD-CT2001-00431 from the EU, and the MAT2001E 4818 and MAT2001 3713-C04-02 Projects. The authors are grateful to Dr A Castro for help in sample preparation and to Dr L Pardo for helpful discussions. R Jiménez acknowledges the Ramon y Cajal Programme of the Spanish MCy T for financial support.

References

[1] Megaw H D 1974 *Ferroelectrics* **7** 87
[2] Von der Mühll R, Sadel A, Ravez J and Hagenmüller P 1979 *Solid State Commun.* **31** 151
[3] Jiménez B, Castro A and Pardo L 2003 *Appl. Phys. Lett.* **82** 3940

[4] Chen J and Feng D 1988 *Phys. Status Solidi* a **109** 171
[5] Sakowski-Cowley A C, Lukaszewicz K and Megaw H D 1969 *Acta Crystallogr.* B **25** 851
[6] Lanfredi S, Lente M H and Eiras J A 2002 *Appl. Phys. Lett.* **80** 2731
[7] Wang C L, Wang Y G, Zhang P L, Zhong W L and Zhao H S 1993 *Solid State Commun.* **85** 331
[8] Zhong W L, Zhang P L, Zhao H S, Yang Z H, Song Y Y and Chen H C 1992 *Phys. Rev.* B **46** 10583
[9] Juang Y D, Dai S B, Wang Y C, Hwang J S, Hu M L and Tse W S 2000 *J. Appl. Phys.* **88** 742
[10] Von der Mühll R, Sadel A and Hagenmüller P 1984 *J. Solid State Chem.* **51** 176
[11] Juang Y D, Dai S B, Wang Y C, Chou W Y, Hwang J S, Hu M L and Tse W S 1999 *Solid State Commun.* **111** 723
[12] Raevski I P and Prosandeev S A 2002 *J. Phys. Chem. Solids* **63** 1939
[13] Castro A, Jiménez B, Hugría T, Moure A and Pardo L 2004 *J. Eur. Electroceram. Soc.* **24** 941
[14] Wang X B, Shen Z X, Hu Z P, Qin L, Tang S H and Kuok M H 1996 *J. Mol. Struct.* **385** 1
[15] Ang C and Yu Z 2000 *Phys. Rev.* B **61** 957
[16] Shen Z X, Wang X B, Kuok M H and Tang S H 1998 *J. Raman Spectrosc.* **29** 279
[17] Bouziane E, Fontana M D and Ayadi M 2003 *J. Phys.: Condens. Matter* **15** 1387
[18] Hafid M, Kugel G E, Kania A, Roleder K and Fontana M D 1992 *J. Phys.: Condens. Matter* **4** 2333
[19] Sokoloff J P, Chase L L and Rytz D 1988 *Phys. Rev.* B **38** 597
[20] Laguna M A and Sanjuán M L 2002 *Ferroelectrics* **272** 63
[21] Lefkowitz I, Lukaszewicz K and Megaw H D 1966 *Acta Crystallogr.* **20** 670
[22] Reznichenko L A, Shilkina L A, Gagarina E S, Raevskii I P, Dul'kin E A, Kuznetsova E M and Akhnazarova V V 2003 *Crystallogr. Rep.* **48** 448
[23] Wells M and Megaw H D 1961 *Proc. Phys. Soc. Lond.* **78** 1258
[24] Glazer A M and Megaw H D 1973 *Acta Crystallogr.* A **29** 489
[25] Zeyfang R R, Henson R M and Maier W J 1977 *J. Appl. Phys.* **48** 3014
[26] Nitta T 1968 *J. Am. Ceram. Soc.* **51** 626
[27] Lima R J C, Freire P T C, Sasaki J M, Ayala A P, Melo F E A, Mendes Filho J, Serra K C, Lanfredi S, Lente M H and Eiras J A 2002 *J. Raman Spectrosc.* **33** 669
[28] Chen I W 2000 *J. Phys. Chem. Solids* **61** 197
[29] Yuzyuk Y I, Gagarina E, Simon P, Reznitchenko L A, Hennet L and Thiaudière D 2004 *Phys. Rev.* B **69** 144105
[30] Raevskii I P, Iliev M P, Reznichenko L A, Palatnikov M N, Balyunis L E and Malitskaya M A 2002 *Tech. Phys.* **47** 772